A neutron diffraction study of structural distortion and magnetic ordering in the cation-ordered perovskites Ba2Nd1−xYxMoO6

ARTICLE *in* JOURNAL OF SOLID STATE CHEMISTRY · APRIL 2013

Impact Factor: 2.13 · DOI: 10.1016/j.jssc.2013.01.023

2 AUTHORS, INCLUDING:

Edmund John Cussen
University of Strathclyde
82 PUBLICATIONS **3,127** CITATIONS

SEE PROFILE

Journal of Solid State Chemistry 200 (2013) 215–220

Contents lists available at SciVerse ScienceDirect

Journal of Solid State Chemistry

journal homepage: www.elsevier.com/locate/jssc

A neutron diffraction study of structural distortion and magnetic ordering in the cation-ordered perovskites $Ba_2Nd_{1-x}Y_xMoO_6$

Oonagh M. Collins, Edmund J. Cussen*

WestCHEM, Department of Pure and Applied Chemistry, University of Strathclyde, Thomas Graham Building, 295 Cathedral Street, Glasgow, G1 1XL, Scotland

ARTICLE INFO

Article history:
Received 7 December 2012
Received in revised form
14 January 2013
Accepted 18 January 2013
Available online 31 January 2013

Keywords:
Perovskite
Neutron diffraction
Magnetic ordering
Cation-doping
Jahn–Teller distortion

ABSTRACT

The cation ordered perovskites $Ba_2Nd_{1-x}Y_xMoO_6$ ($0.04 \le x \le 0.35$) have been synthesised by solid-state techniques under reducing conditions at temperatures up to 1350 °C. Rietveld analyses of X-ray and neutron powder diffraction data show that these compounds adopt a tetragonally distorted perovskite structure. The tetragonal distortion is driven by the bonding requirements of the Ba^{2+} cation that occupies the central interstice of the perovskite; this cation would be underbonded if these compounds retained the cubic symmetry exhibited by the prototypical structure. The size and charge difference between the lanthanides and Mo^{5+} lead to complete ordering of the cations to give a rock-salt ordering of $Nd^{3+}/Y^{3+}O_6$ and MoO_6 octahedra. The $I4/m$ space group symmetry is retained on cooling the $x=0.1$, 0.2 and 0.35 samples to low temperature ca. 2 K. $Ba_2Nd_{0.90}Y_{0.10}MoO_6$ undergoes a gradual distortion of the MoO_6 units on cooling from room temperature to give two long *trans* bonds (2.001(2) Å) along the z-direction and four shorter apical bonds (1.9563(13) Å) in the xy-plane. This distortion of the MoO_6 units stabilises the $4d^1$ electron in the d_{xz} and d_{yz} orbitals whilst the d_{xy} orbital is increased in energy due to the contraction of the Mo–O bonds in the xy-plane. This bond extension along z is propagated through the structure and gives a negative thermal expansion of $-13\times10^{-6}\,K^{-1}$ along c. The overall volumetric thermal expansion is positive due to conventional expansion along the other two crystallographic axes. With increasing Y^{3+} content this distortion is reduced in $x=0.2$ and eliminated in $x=0.35$ which contains largely regular MoO_6 octahedra. The $x=0.1$ and $x=0.2$ show small peaks in the neutron diffraction profile due to long range antiferromagnetic order arising from ordered moments of ca. 2 μ_B.

1. Introduction

Complex perovskite oxides continue to be widely studied as they provide both a source of new physical phenomena and a tuneable system for the development and testing of theory. The incorporation of combinations of cations into the structure can be used to induce chemical ordering and access new electronic states that are not present in the component phases. A classic example of this can be seen by comparing the complexity of the room-temperature magnetoresistive phase [1,2] Sr_2FeMoO_6 with $SrFeO_3$ [3] and $SrMoO_3$ [4,5]. We have been examining related Mo^{5+} perovskites [6] and have seen that in the electronically localised phase Ba_2NdMoO_6 the degeneracy of the $4d^1$ configuration of Mo^{5+} in the octahedral ligand field leads to a distortion and a structural transition from tetragonal to triclinic symmetry at ca. 140(10) K [7]. Cooling this material further leads to antiferromagnetic ordering of both the Nd^{3+} and Mo^{5+} cations at 15 K.

Ba_2SmMoO_6 shows similar structural and electronic behaviour although the temperature dependence is very different [8]. The tetragonal to triclinic distortion occurs at 353 K with no significant distortion of the MoO_6 octahedra. These octahedra undergo distortion over a narrow temperature range close to the Néel temperature of 130 K. Studies of the related compounds Ba_2Ln-MoO_6 have so far suggested that the Nd and Sm compounds are unique in showing this distortion. A detailed study of $Ba_{2-x}Sr_x$ $ErMoO_6$ induced a high temperature structural distortion shown in Fig. 1 that matched that observed in Ba_2NdMoO_6. However, the MoO_6 octahedra in the tetragonal phases of the $Ba_{2-x}Sr_xErMoO_6$ series showed no tendency to distort and no compositions gave the triclinic phase [9].

The cubic phase Ba_2YMoO_6 shows exceptionally strong antiferromagnetic coupling with a Weiss constant of ca. −140 K [6,10–12]. The geometric frustration of the face-centred cubic lattice [13] shown in Fig. 1 prevents long range magnetic order and leads to a novel loss of magnetic moment on cooling due to the formation of a valence bond state [10,12,14]. We have previously established that introducing Y^{3+} into Ba_2NdMoO_6 gives a solid solution that undergoes a transition to a room

* Corresponding author. Fax: +44 141 548 4822.
E-mail address: Edmund.Cussen@strath.ac.uk (E.J. Cussen).

0022-4596/$ - see front matter © 2013 Elsevier Inc. All rights reserved.
http://dx.doi.org/10.1016/j.jssc.2013.01.023

temperature cubic phase for doping levels of $\geq 40\%$ Y substitution [7]. For $x < 0.25$ the series $Ba_2Nd_{1-x}Y_xMoO_6$ show magnetic transitions in the range 10–15 K. In this paper we report a neutron diffraction study of these compounds in order to probe the nature of the low temperature phase. This allows us to identify any distortion of the MoO_6 units and examine the nature of the low temperature magnetic state of these compounds below the transitions observed in the bulk susceptibility measurements.

2. Experimental

Samples were synthesised using conventional solid-state techniques. Stoichiometric mixtures of $BaCO_3$, MoO_3, Nd_2O_3 and Y_2O_3 were mixed and heated at temperatures up to 1350 °C in 5% H_2 in N_2 as described previously [7]. The progress of the reactions was followed using X-ray powder diffraction. After repeated regrinding and repressing of the reaction mixtures and repeatedly heating the samples over between 3 and 5 days at 1350 °C, the diffraction pattern could be completely indexed using a unit cell indicative of a cation-ordered perovskite. Further heating caused no change in the diffraction profile and so indicated that the reaction was complete.

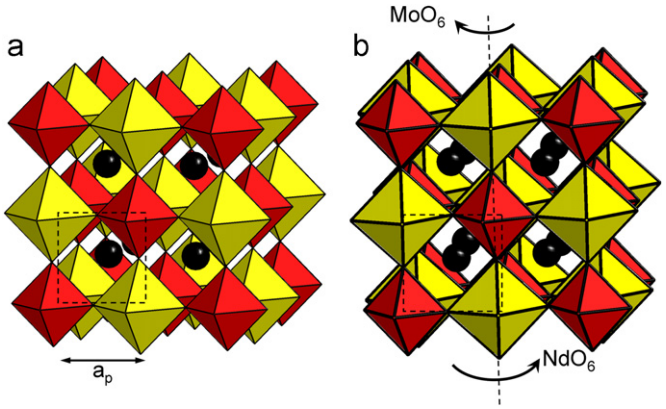

Fig. 1. The crystal structures of (a) Ba_2YMoO_6 (cubic) and (b) $Ba_2NdMoO6$ (tetragonal) [6,10]. Yellow and red octahedra represent Y/NdO_6 and MoO_6 octahedra, respectively. The unit cell of the primitive perovskite substructure is shown as a_p. The subtle structural distortion in (b) is most evident in the rotation of the NdO_6 and MoO_6 units in opposite senses about the fourfold axis represented by a dashed line. (For interpretation of the references to color in this figure caption, the reader is referred to the web version of this article.)

Powder neutron diffraction profiles were measured at various temperatures using the time-of-flight high-resolution powder diffractometer (HRPD), installed at the ISIS spallation source at the Rutherford Appleton Laboratories, Didcot, UK. For this experiment ca. 4 g of sample was housed in a cylindrical vanadium can, with an internal diameter of 11 mm. Diffraction patterns were recorded over the time-of-flight range 30–130 ms in back-scattering, 90° and 30° detector banks, in order to sample a *d*-spacing range from 0.6 to 8 Å. Crystal and magnetic structures were determined using the Rietveld method [15] of structure refinement using the GSAS suite of programs [16]. A shifted Chebyshev function was used to fit the background empirically and a convolution of exponential and pseudo Voigt functions was used to model the profile of the Bragg peaks.

3. Results

Neutron diffraction data collected at room temperature from $Ba_2Nd_{0.96}Y_{0.04}MoO_6$ and $Ba_2Nd_{0.90}Y_{0.10}MoO_6$ can be satisfactorily fitted using the tetragonal space group *I*4/*m* observed in $Ba_2NdMoO6$ at room temperature [6]. Trial refinements showed that the compounds are stoichiometric in oxygen and there is no evidence of site mixing between Mo and Nd/Y. The trivalent charge on Nd/Y and oxide stoichiometry indicates that the molybdenum is present in the 5+ oxidation state. Other studies of the Ba_2LnMoO_6 phases show that these compositions remain stoichiometric in oxide [7,9,11], with any site mixing between the *Ln* and Mo cations reaching a maximum value of ca. 3% that is below the detection limit for typical neutron diffraction data [12]. The structures were refined in a straightforward manner to give the atomic parameters and bond lengths collected in Tables 1 and 2, respectively. Additional datasets were collected from $Ba_2Nd_{0.90}Mo_{0.10}O_6$ at temperatures down to 2 K. The neutron diffraction data collected from this compound at temperatures of 40 K and above can be indexed using the *I*4/*m* space group observed at room temperature, albeit with a considerable expansion of the *c* lattice parameter on cooling the material.

Neutron diffraction data collected from $Ba_2Nd_{0.90}Y_{0.10}MoO_6$ at 15 K and 2 K contained additional peaks at large *d*-spacings that are systematically absent in the body-centred tetragonal cell observed at higher temperatures. As shown in Fig. 2 there was

Table 1
Fit and structural parameters for $Ba_2Nd_{1-x}Y_xMoO_6$ derived from Rietveld refinement against neutron diffraction data.

	$x=0.04$	$x=0.1$							$x=0.2$	$x=0.35$
T/K	293 K	2 K	15 K	40 K	80 K	130 K	160 K	293 K	4 K	4 K
a/Å	6.00797 (6)	5.97254 (4)	5.97323 (9)	5.97301 (9)	5.97492 (12)	5.97715 (13)	5.98120 (9)	6.00592 (7)	5.9700 (1)	5.96158 (12)
c/Å	8.56357 (9)	8.58211 (10)	8.5835 (1)	8.5841 (1)	8.5870 (2)	8.5852 (2)	8.5808 (1)	8.5513 (1)	8.5597 (2)	8.5297 (2)
Vol/Å^2	309.108 (9)	306.135 (5)	306.26 (1)	306.26 (1)	306.55 (2)	306.72 (2)	306.977 (13)	308.455 (11)	305.08 (2)	303.15 (2)
Ba $100U_{11,\ 22}$/Å^2	1.48 (3)	0.10 (4)	0.15 (3)	0.16 (3)	0.13 (3)	0.28 (3)	0.46 (3)	0.04 (3)	0.33 (4)	0.09 (3)
Ba $100U_{33}$/Å^2	1.87 (6)	0.70 (8)	0.59 (6)	0.55 (6)	0.53 (6)	0.85 (7)	1.15 (6)	0.73 (6)	1.25 (7)	1.59 (7)
Mo/Nd/Y $100U_{iso}$/Å^2	1.18 (2)	0.35 (3)	0.36 (2)	0.31 (2)	0.27 (2)	0.36 (2)	0.55 (2)	1.08 (2)	0.66 (2)	0.51 (2)
O (1) z	0.2697 (2)	0.2668 (3)	0.2667 (2)	0.2669 (2)	0.2670 (2)	0.2671 (2)	0.2677 (2)	0.2698 (2)	0.2677 (2)	0.2684 (2)
O (1)$100U_{11,\ 22}$/Å^2	2.85 (5)	1.03 (6)	0.99 (4)	1.04 (5)	0.96 (4)	1.12 (5)	1.25 (4)	2.32 (5)	1.00 (5)	0.42 (5)
O (1)$100U_{33}$/Å^2	1.59 (7)	1.14 (11)	1.18 (9)	1.04 (9)	1.08 (8)	1.23 (9)	1.22 (8)	1.43 (7)	1.7 (1)	2.1 (1)
O (2) x	0.24298 (13)	0.2354 (2)	0.2356 (2)	0.2354 (2)	0.2357 (1)	0.2361 (2)	0.2367 (2)	0.2436 (1)	0.2370 (2)	0.2384 (2)
O (2) y	0.29796 (14)	0.3070 (2)	0.3069 (2)	0.3067 (2)	0.3064 (1)	0.3052 (2)	0.3041 (2)	0.2958 (2)	0.3032 (2)	0.2991 (2)
O (2)$100U_{11}$/Å^2	1.38 (7)	0.43 (9)	0.44 (7)	0.37 (7)	0.45 (7)	0.49 (7)	0.52 (7)	0.59 (6)	0.68 (8)	0.08 (8)
O (2)$100U_{22}$/Å^2	2.29 (6)	1.29 (9)	1.25 (7)	1.09 (6)	1.05 (6)	1.28 (7)	1.34 (7)	2.11 (6)	1.57 (8)	1.49 (8)
O (2)$100U_{33}$/Å^2	3.39 (5)	1.37 (7)	1.34 (5)	1.46 (5)	1.37 (5)	1.54 (6)	1.68 (5)	3.24 (5)	1.81 (6)	2.12 (6)
R_{wp}, χ^2_{red}	5.03, 2.29	4.49, 5.21	3.44, 4.50	3.39, 4.55	3.35, 4.36	3.57, 4.98	3.41, 4.53	5.51, 4.24	3.17, 5.16	3.46, 6.66

Space Group *I*4/*m*: Ba (0, ½, ¼), Mo (0, 0, 1/2), Nd/ Y(0, 0, 0), O(1) (0, 0, *z*), O(2) (*x*, *y*, 0).

Table 2
Bond lengths (Å) and angles (°) of $Ba_2Nd_{1-x}Y_xMoO_6$ derived from Rietveld refinement against neutron diffraction data.

Parameter	$x=0.04$	$x=0.1$							$x=0.2$	$x=0.35$
	293 K	2 K	15 K	40 K	80 K	130 K	160 K	293 K	4 K	4 K
Mo–O (1) × 2	1.9726 (13)	2.001 (2)	2.003 (2)	2.001 (2)	2.001 (2)	2.000 (2)	1.993 (2)	1.9683 (13)	1.988 (2)	1.976 (2)
Mo–O (2) × 4	1.9641 (9)	1.9563 (13)	1.9559 (10)	1.9570 (10)	1.9575 (10)	1.9603 (11)	1.9628 (10)	1.9680 (8)	1.9611 (11)	1.9666 (12)
Nd/Y–O (1) × 2	2.3092 (13)	2.290 (2)	2.289 (2)	2.291 (2)	2.293 (2)	2.293 (2)	2.298 (2)	2.3073 (13)	2.292 (2)	2.289 (2)
Nd/Y–O (2) × 4	2.3099 (9)	2.3103 (13)	2.3109 (10)	2.3095 (10)	2.3097 (10)	2.3066 (11)	2.3050 (10)	2.3022 (8)	2.2975 (11)	2.2800 (12)
Mo–O (2)–Nd/Y	167.37 (4)	163.60 (6)	163.63 (4)	163.66 (4)	163.79 (4)	164.16 (5)	164.55 (4)	167.97 (4)	164.82 (5)	166.08 (5)

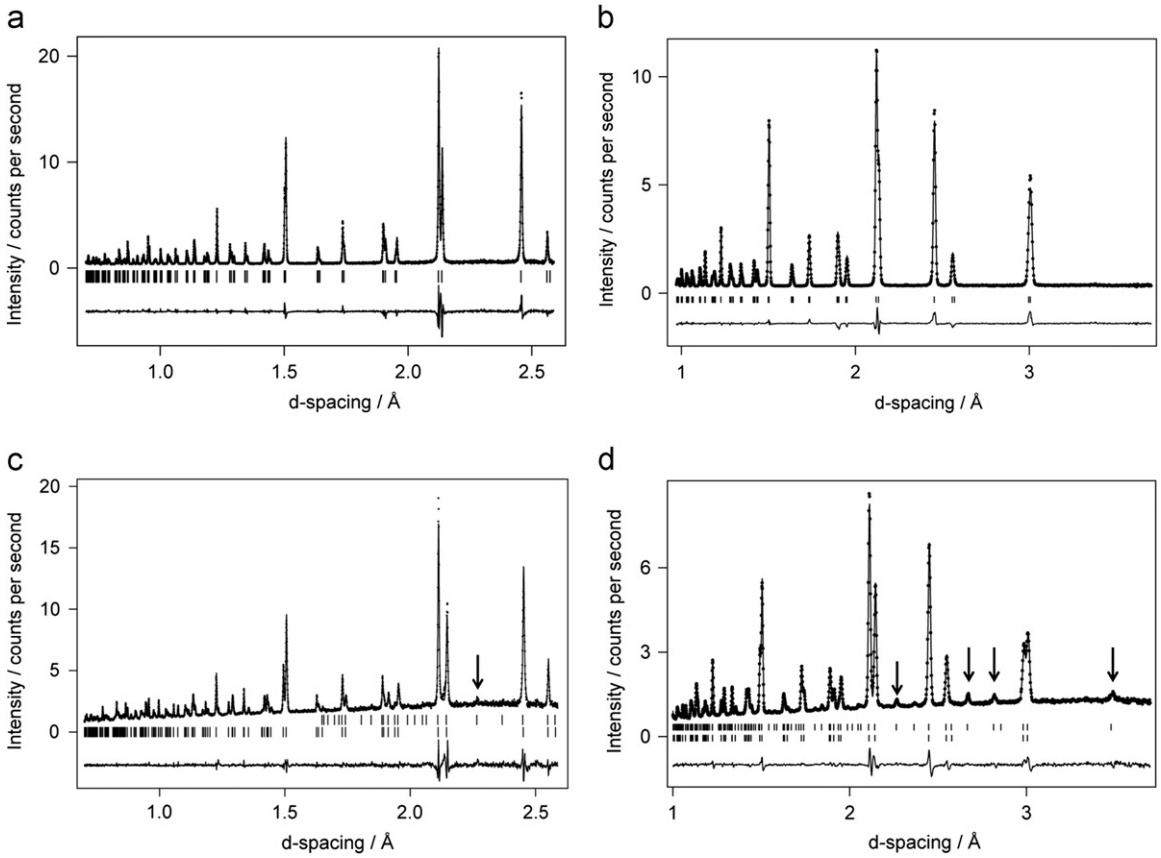

Fig. 2. Neutron diffraction data collected from $Ba_2Nd_{0.90}Y_{0.10}MoO_6$ at (a) and (b) room temperature and (c) and (d) 2 K. The observed, calculated and difference curves are shown by dots and solid lines. The allowed reflections are marked. The magnetic reflections at 2 K are shown by the upper tick marks and the most intense peaks are indicated by arrows.

no significant change in the diffraction pattern at shorter d-spacings indicating that the crystallographic structure was largely unchanged. Magnetisation measurements on this material show a magnetic transition at 15(1) K and the strong temperature dependence of neutron diffraction Bragg peaks around this temperature is indicative of long-range magnetic ordering. These peaks could be indexed using the magnetic model observed in Ba_2NdMoO_6 which contains a primitive magnetic cell of the same dimensions as the nuclear cell, but allows additional reflections due to the loss of the body-centred translational symmetry.

The magnetic scattering in $Ba_2Nd_{0.90}Y_{0.10}MoO_6$ is significantly weaker than in Ba_2NdMoO_6. Ba_2NdMoO_6 contains antiferromagnetically ordered moments on both Nd^{3+} and Mo^{5+} and unconstrained refinement of this magnetic model failed to provide a stable refinement indicating that the data collected from $Ba_2Nd_{0.90}Y_{0.10}MoO_6$ at 2 K only provide information on a single antiferromagnetically ordered moment in the unit cell. The special positions occupied by Nd and Mo in the unit cell mean that it is not possible to identify in *a priori* manner which of the two ions is responsible for the magnetic scattering. However, the moment refines to a value, ca. 2 μ_B, which is too large to arise from scattering from the $S=1/2$, Mo^{5+} ions. The magnetic peaks can be satisfactorily fitted by refining a moment aligned along the *z*-direction of the unit cell which is antiferromagnetically coupled to other magnetic species related by the (1/2, 1/2, 1/2) translation to form ferromagnetically ordered chains that are coupled antiferromagnetically. This structure can be described using the colour spin flips in conjunction with the crystallographic symmetry of the tetragonal space group; namely the fourfold axis (black), the mirror plane (black) and the translational symmetry (red) [17]. This symmetry constrains the magnetic moments to lie along the *z*-direction and allows refinement of moments on both the Nd and Mo positions in the unit cell as indicated in Table 3. The moment refines to a value of 2.90(4) and 2.24(4) μ_B per Nd^{3+} at 2 K and 15 K, respectively. Attempts to refine a moment on the Mo site gave a values of ca. 0.12(4) μ_B that are close to the detection limits of the data and greatly reduced from the anticipated value of $gS=1$ μ_B.

Table 3
Magnetic structure of $Ba_2Nd_{0.90}Y_{0.10}MoO_6$ and $Ba_2Nd_{0.8}Y_{0.2}MoO_6$.[a]

Atom	Atomic coordinates	Magnetic moment 0, 0, m_z (μ_B)		
	x, *y*, *z*	$Ba_2Nd_{0.90}Y_{0.10}MoO_6$		$Ba_2Nd_{0.8}Y_{0.2}MoO_6$
		2 K	**15 K**	**3.5 K**
Nd (1)	0, 0, 0	2.90 (4)	2.24 (4)	2.18 (6)
Nd (2)	1/2, 1/2, 1/2	−2.90 (4)	−2.24 (4)	−2.18 (6)
Mo (1)	1/2, 0, 0	0.11 (3)	0.14 (4)	−0.02 (5)
Mo (2)	0, 1/2, 1/2	−0.11 (3)	−0.14 (4)	0.02 (5)

[a] The magnetic and crystallographic cells have the same dimensions, as shown in Table 1.

Although the structure does not undergo a crystallographic transition there are considerable changes in the structure on cooling. These are most clearly shown in the dimensions of the MoO_6 octahedra and increase in the *c*-parameter on cooling. Fig. 4 shows the variation in the Mo–O bond lengths as a function of temperature in $Ba_2Nd_{0.90}Y_{0.10}MoO_6$.

The same tetragonal model was used to fit data collected from $Ba_2Nd_{0.80}Y_{0.20}MoO_6$ at 4 K. These data contained similar Bragg peaks at high d-spacing indicative of long-range antiferromagnetic ordering and refinement of the magnetic model gave an ordered moment of 2.18 (6) μ_B per Nd^{3+} and −0.02 (5) μ_B per Mo^{5+}. The tetragonal nuclear structure is preserved in $Ba_2Nd_{0.65}Y_{0.35}MoO_6$ but the magnetic Bragg peaks are absent in data collected at 4 K as shown in Fig. 3. Structural parameters and bond lengths from all of these refinements are collected in Tables 1 and 2, respectively.

4. Discussion

Neutron diffraction data have provided a full crystallographic description of compounds in the series $Ba_2Nd_{1-x}Y_xMoO_6$ that confirms that these phases are tetragonal at low temperature for $0.10 \le x \le 0.35$. This distortion is driven by the bonding requirements of the large Ba^{2+} cation that occupies the central interstice of the cubic perovskite structure. Whereas Ba_2YMoO_6 is cubic, Ba_2NdMoO_6 is distorted in order to maintain acceptable distances between the Ba^{2+} cation and the oxide anions. At room temperature $Ba_2Nd_{0.90}Y_{0.10}MoO_6$ shows a range of Ba–O distances of 4×2.8662 (5), 4×3.00774 (8) and 4×3.1782 (6) Å giving a total bond valence of 1.91 [18].

If $Ba_2Nd_{0.90}Y_{0.10}MoO_6$ were to form a cubic perovskite with the same mean Mo–O and Nd/Y–O distances observed in the tetragonal room temperature phase this would give a face-centred cubic structure with a lattice parameter of $2 \times \langle Mo\text{–}O \rangle + 2 \times \langle Nd/Y\text{–}O \rangle = 8.54487$ Å. The resultant 12 Ba–O bond lengths of 3.0258 Å would give an unacceptably low value for the bond valence of 1.66 indicating that Ba^{2+} would be underbonded in this hypothetical structure. The observed distortion increases the bond valence for Ba^{2+} but both the MoO_6 and Nd/YO_6 octahedra remain largely regular at room temperature despite the reduction to tetragonal symmetry.

On cooling $Ba_2Nd_{0.90}Y_{0.10}MoO_6$ the MoO_6 octahedra undergo an elongation of the apical Mo–O bonds. This is accompanied by a smaller contraction of the four equatorial distances so that by 2 K these bond lengths are 2.001 (2) and 1.9563 (13) Å, respectively. All other bond lengths in the structure show the expected contraction on cooling and there are no significant changes in bond angles. Consequently the extension of the apical Mo–O distance is propagated through the structure and leads to negative thermal expansion of $-13 \times 10^{-6}\,K^{-1}$ along the *c*-direction

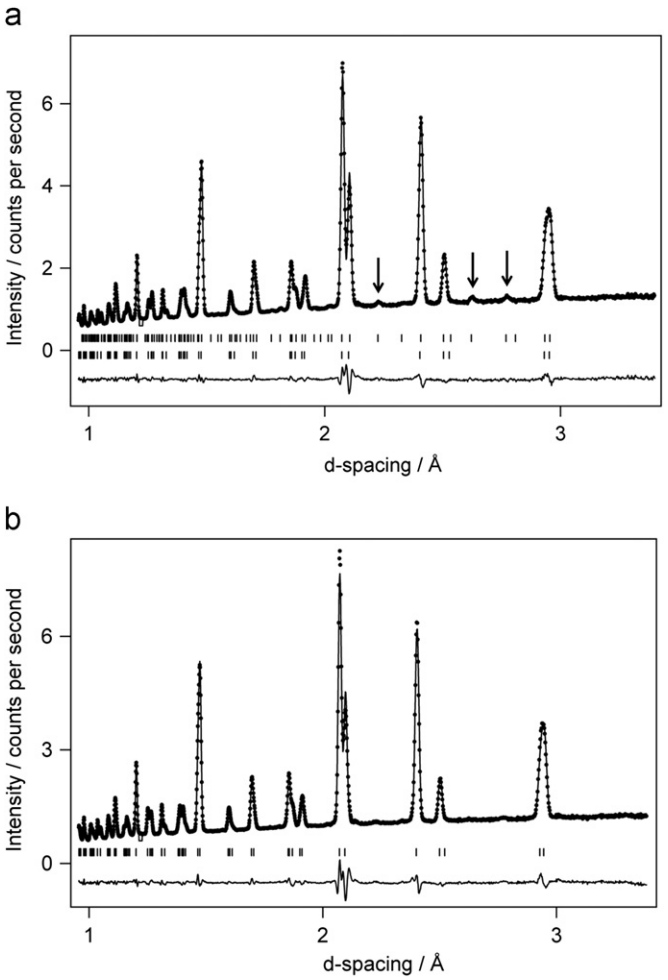

Fig. 3. Neutron diffraction data collected from (a) $Ba_2Nd_{0.80}Y_{0.20}MoO_6$ and (b) $Ba_2Nd_{0.65}Y_{0.35}MoO_6$ at 4 K. The magnetic reflections are indicated in (a) by the upper set of tick marks.

of the unit cell as shown in Fig. 4. This contraction along *c* is insufficient to offset the positive thermal expansion in the *ab*-plane and so this phase exhibits the overall positive volumetric thermal expansion shown in Fig. 4.

Distortions of similar size have arisen in other d^1 systems, such as $NaTiO_2$, [19] where a Jahn–Teller distortion leads to a reduction in the electronic energy by distortion of the ligand field. As there is no change in symmetry on cooling $Ba_2Nd_{0.90}Y_{0.10}MoO_6$ the degeneracy is not lifted. However, the distortion of the MoO_6 units is greatly increased and this stabilises the $4d^1$ electron in the d_{xz} and d_{yz} orbitals whilst the d_{xy} orbital is increased in energy due to the contraction of the Mo–O bonds in the *xy*-plane. The behaviour of $Ba_2Nd_{0.90}Y_{0.10}MoO_6$ differs from the related molybdate phases [7,8] Ba_2NdMoO_6 and Ba_2SmMoO_6 in that it retains the tetragonal symmetry; Ba_2NdMoO_6 and Ba_2SmMoO_6 show a slightly larger distortion with bond lengths of ca. 2.01 and 1.95 Å in structures which have undergone a crystallographic transition to a triclinic phase ($I\bar{1}$).

$Ba_2Nd_{0.80}Y_{0.20}MoO_6$ and $Ba_2Nd_{0.65}Y_{0.35}MoO_6$ have the same tetragonal symmetry as $Ba_2Nd_{0.90}Y_{0.10}MoO_6$ at low temperature but the magnitude of the MoO_6 distortion reduces with increasing Y-content as shown in Fig. 5. In $Ba_2Nd_{0.80}Y_{0.20}MoO_6$ at 4 K the difference in Mo–O distances has reduced to 0.027 (2) Å and in $Ba_2Nd_{0.65}Y_{0.35}MoO_6$ the MoO_6 octahedra are largely regular.

The unambiguous observation of long-range antiferromagnetic order in $Ba_2Nd_{0.90}Y_{0.10}MoO_6$ and $Ba_2Nd_{0.80}Y_{0.20}MoO_6$ shows that

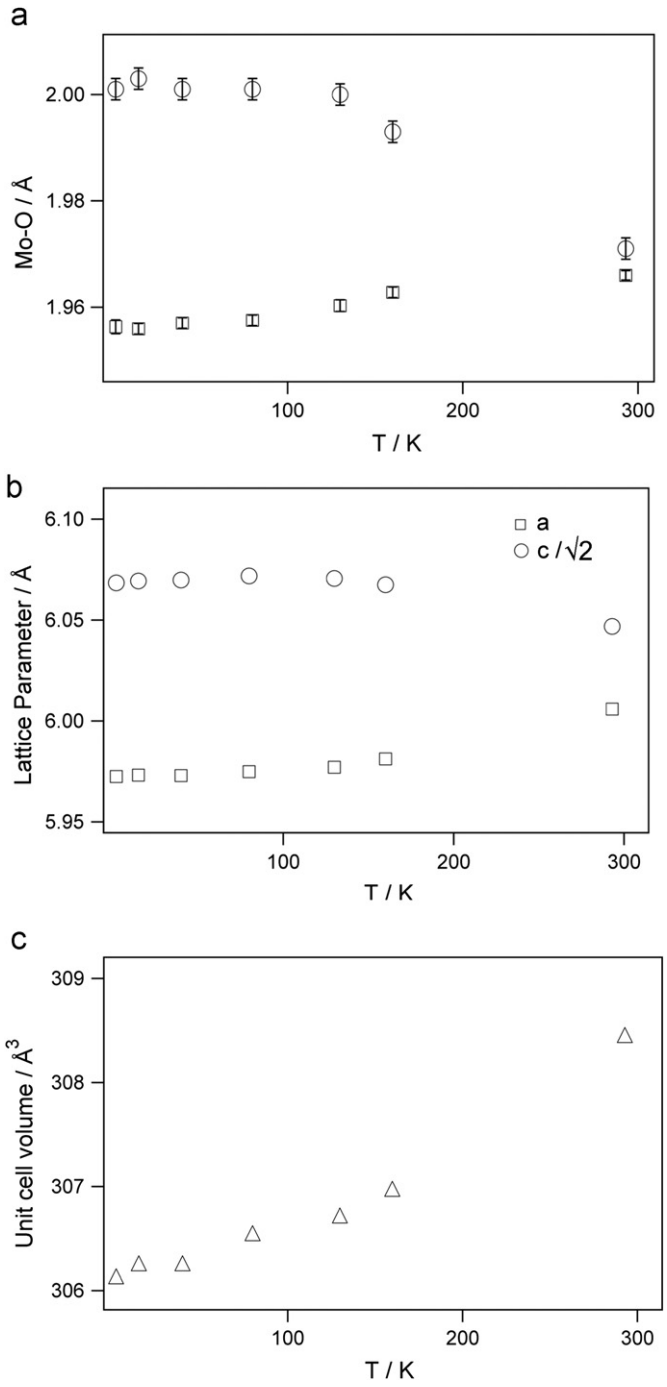

Fig. 4. The variation in (a) Mo-O distances, (b) lattice parameters, and (c) cell volume in $Ba_2Nd_{0.90}Y_{0.10}MoO_6$ as a function of temperature. The error bars in Mo-O distances indicate one standard deviation in the refinement against neutron diffraction data. The small standard deviations reflect the precision afforded by the excellent resolution of the neutron diffraction data and the high space group symmetry. The standard deviation in the lattice parameters is smaller than the symbols.

the distortion of the Mo^{5+} coordination environment in these phases is sufficient to stabilise the anisotropic antiferromagnetic structure observed in Ba_2NdMoO_6. In the absence of this distortion of the MoO_6 octahedra, related tetragonal phases in the $Ba_{2-x}Sr_xErMoO_6$ series remain paramagnetic to 2 K [9]. The reduction in the magnitude of the MoO_6 distortion associated with the replacement of Nd^{3+} with Y^{3+} reduces the size of the ordered magnetic moments gradually with composition. We can thus assign the magnetic transitions observed in the bulk

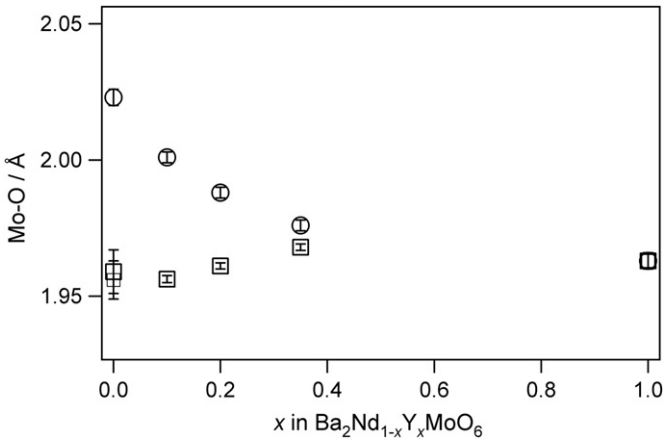

Fig. 5. The variation in Mo–O distances as a function of composition in $Ba_2Nd_{1-x}Y_xMoO_6$ derived from neutron diffraction data collected at 2 or 4 K. Values for Ba_2NdMoO_6 and Ba_2YMoO_6 are taken from the literature [6,10]. Error bars indicate one standard deviation derived from the Rietveld refinement.

susceptibility data [7] to Néel transitions rather than the formation of disordered spin glass states.

The Néel temperature of Ba_2NdMoO_6 is 15 (1) K and so the observation of magnetic Bragg peaks at 15 K in $Ba_2Nd_{0.90}Y_{0.10}MoO_6$ shows that the Néel temperature is unchanged by the introduction of 10% Y^{3+} into the superexchange pathway. Combined with the observation that the ordered moment per Nd^{3+} in $Ba_2Nd_{0.80}Y_{0.20}MoO_6$ is similar to $Ba_2Nd_{0.90}Y_{0.10}MoO_6$ this implies that strength of the magnetic exchange within the ordered portion of the material is not significantly diminished from Ba_2NdMoO_6.

5. Conclusion

The structural chemistry of $Ba_2Nd_{1-x}Y_xMoO_6$ has been examined in detail and shows that Mo^{5+} can drive unusual bonding and magnetic behaviour in this solid solution. Neutron powder diffraction data collected from $Ba_2Nd_{0.90}Y_{0.10}MoO_6$ between room temperature and 2 K show that the MoO_6 octahedra undergo a gradual extension of the Mo–O apical bond. In contrast to Ba_2NdMoO_6 the symmetry remains tetragonal over the whole temperature range. Long range antiferromagnetic order persists with increasing Y^{3+} doping up to $Ba_2Nd_{0.80}Y_{0.20}O_6$. This compound shows a greatly reduced distortion of the MoO_6 units. The distortion disappears along with the antiferromagnetic ordering in $Ba_2Nd_{0.65}Y_{0.35}MoO_6$ which shows a largely regular molybdenum coordination environment despite the presence of a tetragonal symmetry.

Acknowledgments

This work was funded by The Royal Society, EPSRC and the University of Strathclyde. We are grateful to Dr. Aziz Daoud-Aladine for assistance with the neutron diffraction experiments and to the Rutherford Appleton Laboratories for providing access to the ISIS neutron source.

References

[1] F. Galasso, F.C. Douglas, R. Kasper, J. Chem. Phys. 44 (1966) 1672.
[2] K.I. Kobayashi, T. Kimura, Y. Tomioka, H. Sawada, K. Terakura, Y. Tokura, Phys. Rev. B 59 (1999) 11159.
[3] J.B. MacChesney, R.C. Sherwood, J.F. Potter, J. Chem. Phys. 43 (1965) 1907.
[4] L.H. Brixner, J. Inorg. Nucl. Chem. 14 (1960) 225.

[5] S. Hayashi, R. Aoki, T. Nakamura, Mater. Res. Bull. 14 (1979) 409.
[6] E.J. Cussen, D.R. Lynham, J. Rogers, Chem. Mater. 18 (2006) 2855.
[7] E.J. Cussen, W.J. Cameron, J. Mater. Chem. 20 (2010) 1340.
[8] A.C. Mclaughlin, Phys. Rev. B 78 (2008) 132404.
[9] E.J. Cussen, J. Solid State Chem. 180 (2007) 474.
[10] M.A. de Vries, A.C. McLaughlin, J.W.G. Bos, Phys. Rev. Lett. 104 (2010) 177202.
[11] A.C. Mclaughlin, Solid State Commun. 137 (2006) 354.
[12] T. Aharen, J.E. Greedan, C.A. Bridges, A.A. Aczel, J. Rodriguez, G. MacDougall, G.M. Luke, T. Imai, V.K. Michaelis, S. Kroeker, H.D. Zhou, C.R. Wiebe, L.M.D. Cranswick, Phys. Rev. B 81 (2010) 224409.
[13] J.E. Greedan, in: D.W. Bruce, D. O'Hare, R.I. Walton (Eds.), Functional Oxides, John Wiley & Sons, Ltd., Chichester, 2010, p. 41.
[14] A.C. McLaughlin, M.A. de Vries, J.W.G. Bos, Phys. Rev. B 82 (2010) 094424.
[15] H.M. Rietveld, J. Appl. Crystallogr. 2 (1969) 65.
[16] A.C. Larson, R.B. von Dreele, General Structure Analysis System (GSAS); Los Alamos National Laboratories: Los Alamos, NM, 1990.
[17] J. Cui, Q. Huan, B.H. Toby, Powder Diffr. 21 (2006) 71.
[18] N.E. Brese, M. O'Keeffe, Acta Cryst. B47 (1991) 192.
[19] S.J. Clarke, A.J. Fowkes, A. Harrison, R.M. Ibberson, M.J. Rosseinsky, Chem. Mater. 10 (1998) 372.